Supporting Information

Mn_3O_4@CoHCF nanocomposite for charge transfer regulated kinetic degradation of organophosphate pesticides

Mahima Singh[1], Manviri Rani[1*], Uma Shanker[2*]

[1]Department of Chemistry, Malaviya National Institute of Technology Jaipur, Rajasthan-302017-INDIA

[2]Department of Chemistry, Dr B R Ambedkar National Institute of Technology Jalandhar, Punjab, India-144008

* Corresponding Author

Dr Manviri Rani
Analytical Research Laboratory
Department of Chemistry
Malaviya National Institute of Technology Jaipur,
Rajasthan, India
Email: manviri.chy@mnit.ac.in
Contact number: +91- 9549650291

Dr Uma Shanker
Nanomaterials green synthesis laboratory
Department of Chemistry
Dr B R Ambedkar National Institute of Technology Jalandhar, Punjab -India

Email: shankeru@nitj.ac.in
Contact number: +91-7837588168

Text S1. Information on chemicals, and solvents used in this study

All reagents and materials used in this study were of analytical grade and used as received without further purification. Ethion (ET 99.99%) and Chlorpyrifos (CP 99.99%) were supplied by Sigma-Aldrich (Merck, India). Sodium Hydroxide (98% purity), Manganese (II) Chloride Tetrahydrate 98% AR purchased from LOBA Chemie, India. Potassium Ferrocyanide[$K_4Fe(CN)6$] 99% purity, Cobaltous Chloride Hexahydrate ($CoCl_2$.6H2O) 98% purity were purchased from RANKEM, India. For Scavenger analysis, tert-butyl hydroxide (t-BuOH, 98.9%), and chloroform ($CHCl_3$ 98.9%) and Ethylene diamine tetra acetic acid salt (EDTA) were brought from Rankem Chemical (Savita Scientific, Jaipur). Aloevera leaves were collected locally from MNIT Campus, Jaipur.

Preparation details of plant extract:

Plant extract of Aloevera was prepared by firstly removing the rind and outer layer from the leaf, and extract the gel from the leaves using various method like scraping. Deionized water was used throughout the experiment.

Role of Plant extract

In the present work, the use of *Aloe vera* extract in the synthesis of the Mn_3O_4@CoHCF nanocomposite provides a dual functional role as both a reducing and stabilizing agent, owing to its rich phytochemical composition. The extract contains polyphenolic compounds, particularly anthraquinones (e.g., aloin and aloe-emodin) and flavonoids, which possess redox-active hydroxyl and carbonyl groups capable of donating electrons to facilitate the reduction of precursor metal ions during nanocomposite formation. Concurrently, naturally abundant polysaccharides (such as acemannan), along with proteins and saponins, contribute to effective surface capping and stabilization through hydrogen bonding and electrostatic interactions, thereby preventing nanoparticle agglomeration and controlling growth kinetics. Additionally, minor constituents such as ascorbic acid further enhance the reduction process. Collectively, these biomolecules enable a green, sustainable synthesis pathway, promoting the formation of a well-dispersed and structurally stable Mn_3O_4@CoHCF heterostructure with improved

interfacial contact, which is advantageous for enhanced charge separation and photocatalytic performance.

Text S2: Instrumentation

The samples were subjected to PXRD analysis using CuKa radiation with λ = 1.5406 A and a PAN analytical X-PRT PRO system from the USA. Samples that had been adequately ground and evenly distributed were placed in a coplanar form inside the sample container. A number of functional groups and bonds formed in the doped nanocomposite with full scan from 400-4000 cm^{-1} had been confirmed by FT-IR analyses conducted with an Agilent Cary 630 FTIR spectrometer (USA). This method doesn't require any special sample preparation or reference material, in contrast to normal FT-IR, which uses KBr as a reference. A FEI-Nova Nano SEM 450 microscope with a field emission gun was used to assess the surface morphology of the generated samples (Kensington UNSW Sydney, NSW 2052). It gives a resolution of 1.6 nm at 1 kv (TLD-SE) & <1 nm at 15 kv (TLD-SE). Electron dispersive spectroscopy was used to assess the element weight percentage in the sample. The EI ion source has been configured to operate at 350 degrees. An X-ray photoelectron spectroscopy (XPS) measurement was conducted using Oxford instrumentation. The Malvern Zetasizer (Version 7.11) was used to measure the zeta potential in order to evaluate the stability of the photocatalyst. The band gap has been determined by converting the Diffuse Reflectance Spectra data from a Shimadzu UV-Vis spectrometer to Tauc's plot. A UV Spectrophotometer (Agilent Pro) was used to measure the absorbance of the samples within the wavelength of 200−800 nm. The EIS study was conducted by CHI 7087E instrument with frequency range 0.01Hz to 105 Hz at the amplitude of 0.01 V. In addition, CPA-225D Sartius Analytical balance was used for weighing purpose and LABWAN –PH-61WW instruments was used for the preparation of pH solutions total organic carbon (TOC) analysis by the TOC -L analyser Shimazu.

Text S3: Band Gap Calculation

Band gap energy (Eg) was calculating using Tauc eq.

$$\alpha = \frac{C(h\nu - E_g)^n}{h\nu}$$

It is based on Tauc's relation which links the absorption coefficient to the photon energy that serves as the basis for it: $(\alpha h\nu)^2$ $(eV\ cm^{-1})^2$ vs Energy ($h\nu$).

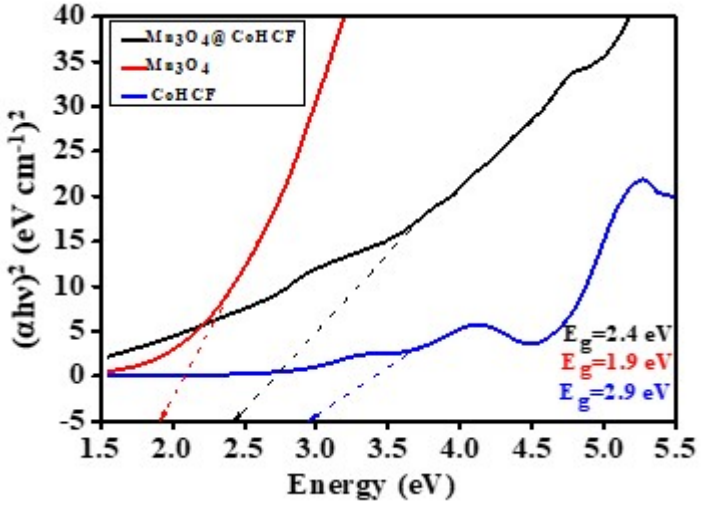

Fig.1S Band Gap analysis of Mn_3O_4@CoHCF, CoHCF and Mn_3O_4

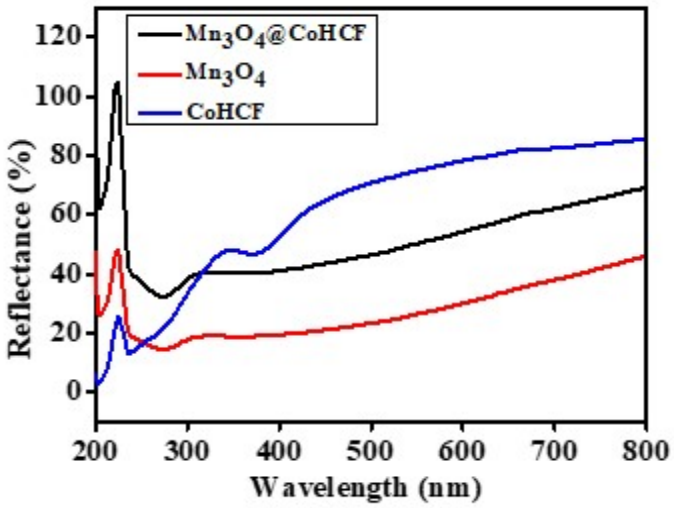

Fig.2S Reflectance spectra of Mn_3O_4@CoHCF, CoHCF and Mn_3O_4

Crystalline size can be calculated using the Scherrer equation i.e.

$$d = \frac{k\lambda}{\beta cos\theta} \qquad (Eq1S)$$

where k is constant and its value is 0.9

λ is X-ray wavelength = 1.5 for Cu

β is the FWHM of the peak profile

θ is the diffraction angle of the reflection

The average crystallite size of Mn_3O_4@CoHCF, Mn_3O_4 and CoHCF is 16.89 nm, 8.39 nm and 11.18 nm, respectively.

Peak broadening and shifting indicated both the strain related to powder and the refinement of the crystal lattice. The following formula was used to determine the strain caused by crystal distortion and imperfection in powder:

$$\delta = 1/D^2 \qquad \text{(Eq 2S)}$$

$$\beta_{hkl} = \frac{K\lambda}{D\cos\theta} + 4\epsilon\tan\theta \qquad \text{(Eq 3S)}$$

Where, K = shape factor (0.9), ε = micro-strain, δ = dislocation density, and λ = wavelength of Cuk radiation (0.154 nm). Plotting between 4 sinθ and β hkl cosθ provides crystalline size (intercept) and micro-strain (slope) from eq.2S. The dislocation density for the nanocomposite was calculated by eq. 3S.

Text S4: Statistical analysis

Sigma plot ver. 10.0 software (SPSS) was used to empirically analyze the reaction kinetics, rate constants, and best fit plots for eliminating Ethion and Chlorpyrifos from nanocatalyst surfaces. The standard deviation was computed using the Microsoft Excel program, which produces higher accuracy with triplicate samples. The results were then supported by Regression of coefficient (R^2) and p- value (≥ 0.05). For adsorption data analysis, several models were used (Langmuir isotherm, Freundlich, Dubinin-Radushkevich (DRK) and Temkin

isotherm). Linear curves(Y=mX+c) for adsorption and concentration-dependent study have been obtained while exponential graphs attaining maxima were observed for reduction.

The pollutant was removed by adsorption over a 60-minute period during the kinetic examination of negative time values. Therefore, the total removal of pesticides consisted of the contributions from both the adsorption and the photodegradation. The details of the adsorption experiment are given below-

The 20 mg of each adsorbent (Mn_3O_4@CoHCF, Mn_3O_4, and CoHCF) was brought into contact with aq. Pesticides solution (50 mg L^{-1}) at 7 pH and reaction mixture was agitated at a speed of 300 rpm for 0-60 min under dark conditions. The percentage of pesticides in each of the aliquot samples was determined after 15, 30, 45, and 60 min by measuring the difference in absorbance using HPLC (Model: 1260WD).

Details of Langmuir, Freundlich, Temkin, Sip and D-R isotherms used in present study

The absorbance (X_e) was calculated through the equation (Figure 4S):

$$X_e = \frac{(Ci - Ce) \times Vol\ of\ solution\ (mL) \times Molecular\ weight\ of\ adsorbent}{Amount\ of\ catalyst\ (mg)}$$

Where C_i and C_e are the initial and the equilibrium concentrations of pesticides in mg L^{-1}; X_e is the amount of EDCs adsorbed per gm weight of adsorbent (photocatalyst).

Adsorption data through Langmuir adsorption isotherms were calculated through a graph of Ce/Xe v/s Ce of the solute. These were calculated by fitting the adsorption data into the equation:

$$\frac{C_e}{X_e} = \frac{1}{k_L X_m} + \frac{C_e}{X_m}$$

or

$$\frac{1}{X_e} = \frac{1}{C_e}\left(\frac{1}{k_L X_m}\right) + \frac{1}{X_m}$$

Freundlich Isotherm.

A typical graph of Xe v/s Ce of the solute was a straight line. $Xe = Kf + Ce1/n$ and the linear form is $$\log Xe = \log Kf + \frac{1}{n} logCe$$

Where C_e is the equilibrium concentration of the VOCs solution; X_e is the number of VOCs adsorbed per gram weight of adsorbent; Kf is the Freundlich adsorption constant (mg g^{-1}); n is adsorption intensity.

Temkin Isotherm:

$$Xe = \frac{RT}{b} \ln A + \frac{RT}{b} \ln Ce$$

Where B=RT/b constant related to heat of sorption (J/mol) obtained from the Temkin plot (qe Vs ln Ce); A (slope) = Temkin isotherm equilibrium binding constant (L g^{-1}); b (intercept) = Temkin isotherm constant; R =universal gas constant (8.314 J mol^{-1} K^{-1}) T = Temperature at 298, 308 and 318 K.

As C_e values were very low, the ln C_e values were coming out to be negative. Therefore, Temkin isotherm (X_e v/s ln C_e) was not plotted for the present study.

Dubinin-Radushkevich (D-R) isotherm:

$$\ln Xe = \ln Xm - \beta\varepsilon 2$$

$$\varepsilon = RT\, ln\left(1 + \frac{1}{Ce}\right)$$

Where X_m is the maximum adsorption capacity (mg g^{-1}) obtained from intercept; β (mol^2J^{-2}) is an activity coefficient constant related to adsorption energy and obtained from slop; ε is Polanyi potential. D-R was plotted between ln Xe Vs ε^2.

Sips Isotherm

It is plotted between 1/Xe $\times 10^{-2}$ (g mg^{-1}) and (1/Ce) $\times 10^{-8}$ L mg^{-1}; where (1/mg) and (mg/g) are the Sips equilibrium constant and maximum adsorption capacity values obtained from the slope and the intercept of the plot. The Sips isotherm equation is characterized by the dimensionless

heterogeneity factor ‘n’ which can also be employed to describe the system’s heterogeneity when is between 0 and 1.

$$\frac{1}{X_e} = \frac{1}{Xm\ Ks}\left(\frac{1}{Ce}\right)1/n + \frac{1}{X_m}$$

Therefore, different adsorption isotherms (Langmuir, Sips, Freundlich, Dubinin-Radushkevich, and Temkin) were investigated. Pesticides eradication was found to be initial adsorption which best fitted the Langmuir adsorption model. The photocatalytic process roughly followed first-order kinetics, which can be expressed as follows: $(C_t/C_0) = \exp^{-kt}$, where |k| is the apparent rate constant and C_t and C_0 are the final and initial concentrations of VOCs, respectively. Both rate constant and rate suggest that pesticides removal was much faster in sunlight than dark i.e., photodegradation>>>adsorption. Additionally, nanocomposite shows much more photocatalytic activity compared to individual nanoparticles i.e., Mn_3O_4@CoHCF > CoHCF>Mn_3O_4.

Text S5: Turn over frequency (TOF)

As we know that TOF of catalysts determines their efficiency, i.e. higher the TOF more efficient is the catalyst. TOF value can be calculated with the help of following formula:

$$\text{TOF} = \frac{No\ of\ moles\ of\ reactant/No\ of\ grams\ of\ photocatalysts}{Time\ (min)} \times yield$$

No of gram of photocatalyst: 0.02 g. (2ppm)

Table 1S: TOF of Mn_3O_4@CoHCF > CoHCF>Mn_3O_4 for ET and CP pollutants

S.No.	Photocatalyst	TOF (mol min^{-1} g^{-1})	
		ET	CP
1.	Mn_3O_4@CoHCF	1.28×10^{-3}	6.26×10^{-4}
2.	CoHCF	1.16×10^{-3}	5.60×10^{-4}
3.	Mn_3O_4	1.04×10^{-3}	5.06×10^{-4}

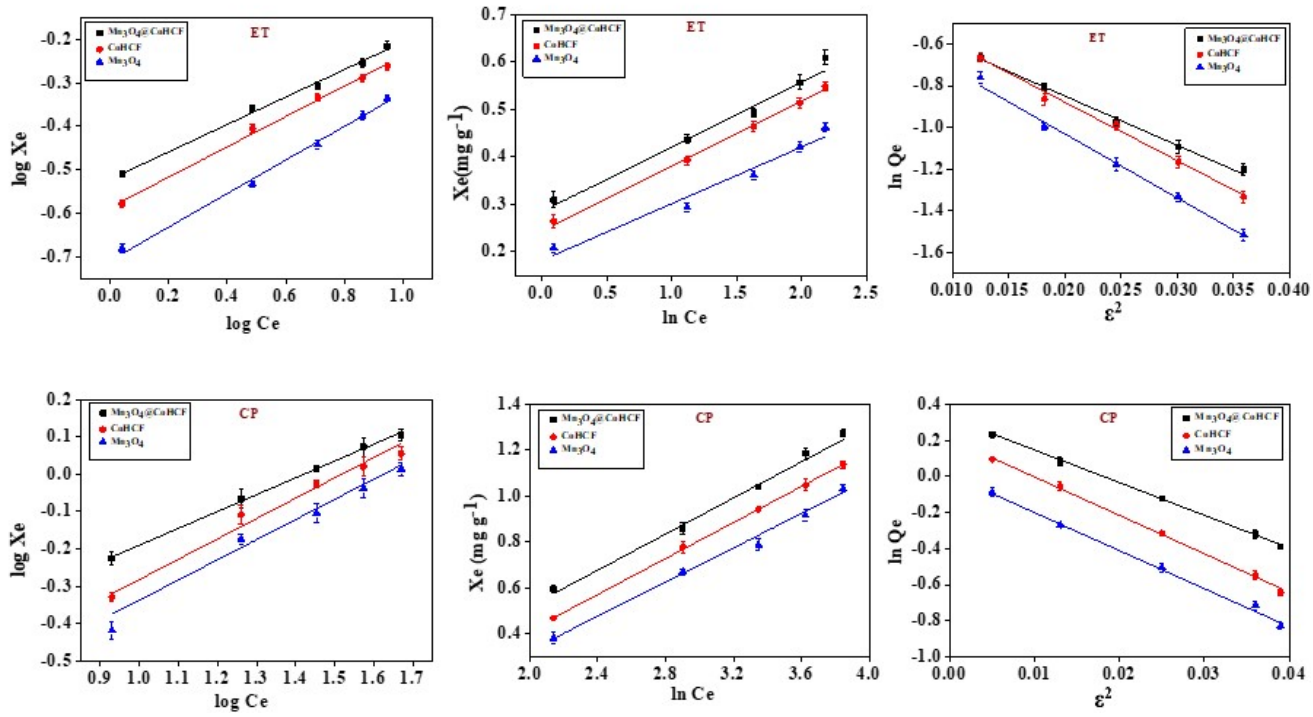

Figure 3S: (a) Freundlich (b) Temkin and (c) D-R isotherms for ET and CP adsorption. Note: Triplicate experiments (n=3) were evaluated for estimation of error bar.

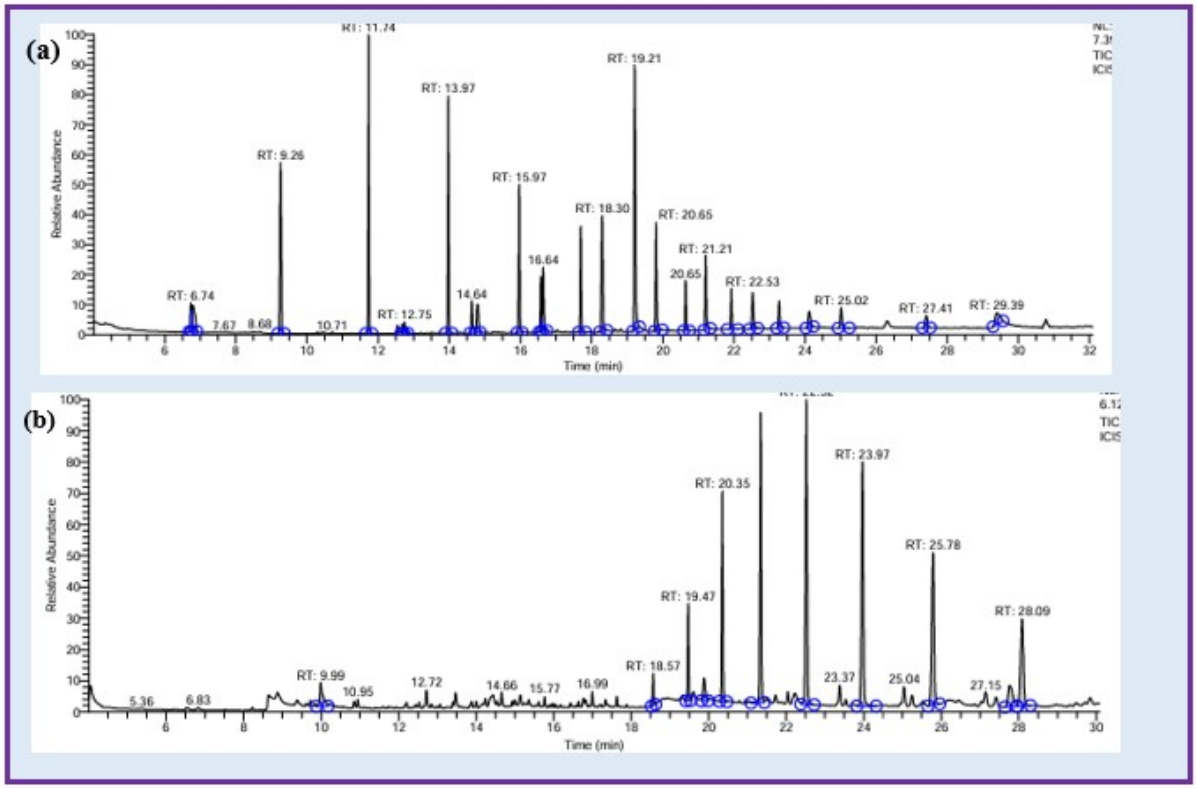

Figure 4S: Representative of Total ion chromatogram (TIC) of (a) Ethion and (b) Chlorpyrifos

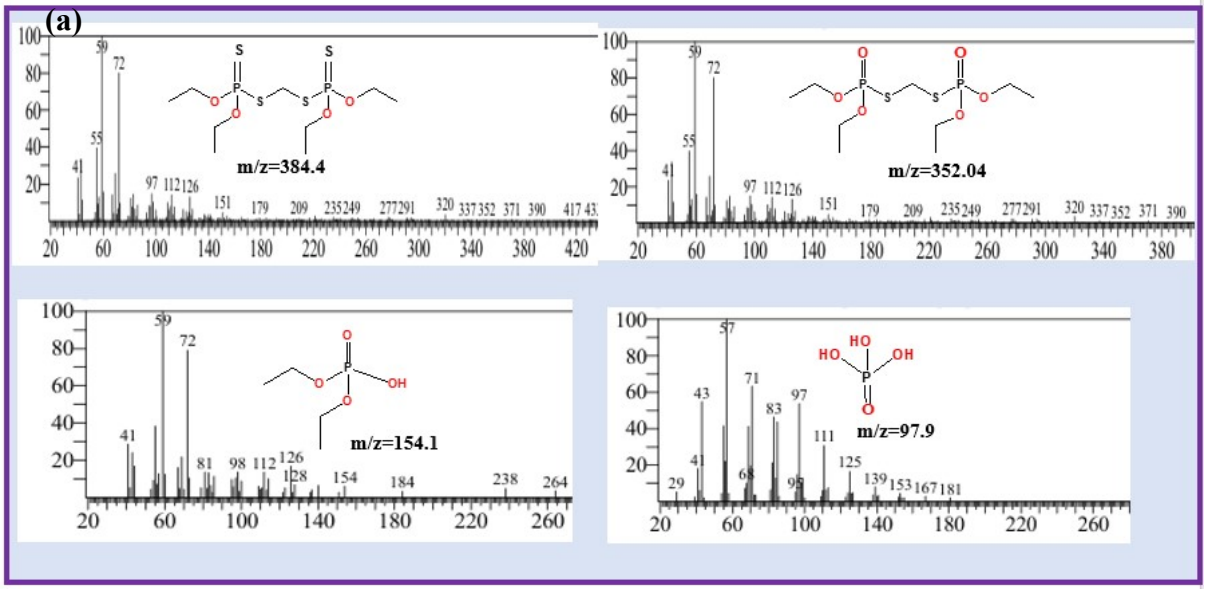

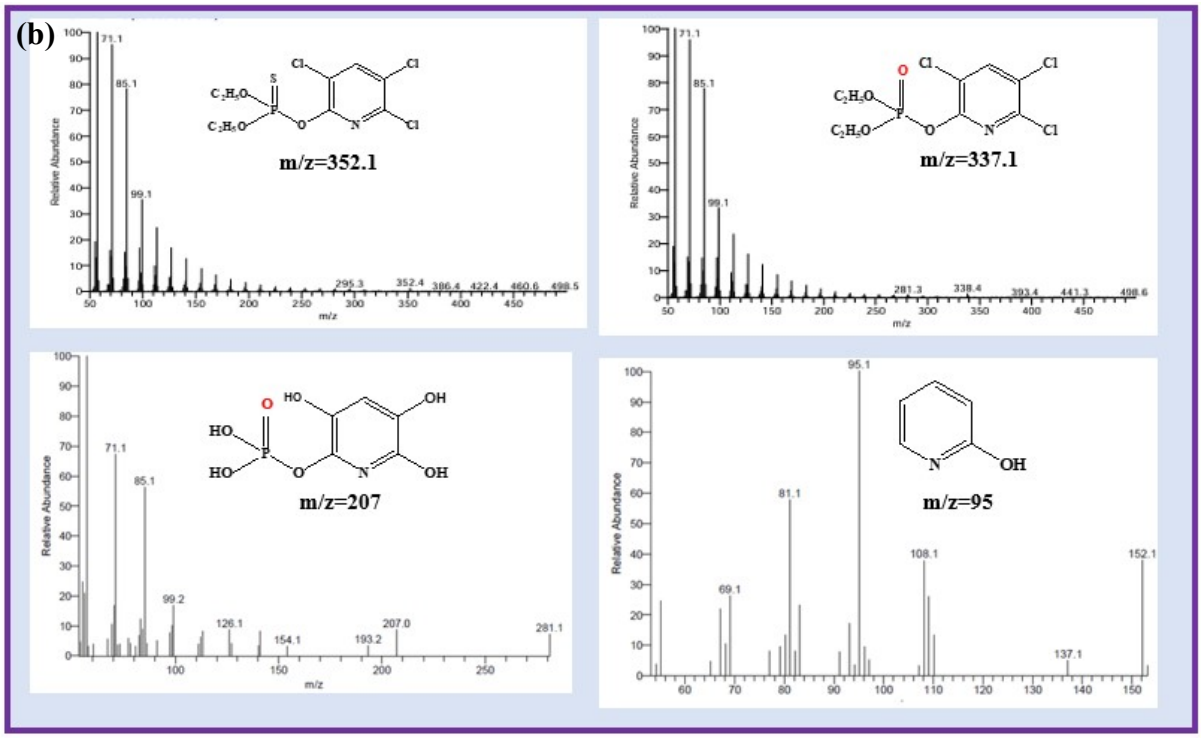

Figure 5S: mass spectrum of the degraded products formed of (a)Ethion and (b) Chlorpyrifos over Mn_3O_4@CoHCF nanocatalysts

Table 2S. Details of angle, FWHM values, interplanar spacing and hkl values of respectively Mn_3O_4@CoHCF, Mn_3O_4 and CoHCF respectively.

a)Mn_3O_4@CoHCF

Angle (2θ)	**FWHM Value**	**d-spacing (Å)**	**hkl values**
19.24º	0.4684	4.59 Å	(101)
29.21º	0.4015	3.06 Å	(112)
32.53º	0.4015	2.74 Å	(103)
36.75º	0.1004	2.47 Å	(211)
38.16º	0.5353	2.35 Å	(004)
51.18º	0.8029	1.78 Å	(440)
60.14º	0.5348	1.53 Å	(224)
64.70º	0.8029	1.43 Å	(314)

B) Mn_3O_4

Angle (2θ)	**FWHM Value**	**d-spacing (A^0)**	**hkl values**
18.14º	0.2676	4.88 Å	(101)
29.10º	0.3011	3.06 Å	(112)
36.75º	0.2007	2.48 Å	(103)
44.54 º	0.3346	2.03 Å	(211)
58.61º	0.5353	1.57 Å	(224)
60.15º	0.4015	1.53 Å	(314)

c) CoHCF

Angle (2θ)	**FWHM Value**	**d-spacing (Å)**	**hkl values**
17.92º	0.1004	4.94 Å	(101)
29.11º	0.1338	3.51 Å	(200)
36.03º	0.1506	2.49 Å	(220)
58.31º	0.2676	1.58 Å	(400)
60.05º	0.4015	1.76 Å	(422)
64.94º	0.1706	1.54 Å	(440)

Table 3S. Comparison of different isotherms on the basis of R^2 and p values for ET and CP adsorption

	Langmuir				**Temkin**			
	ET		**CP**		**ET**		**CP**	
Catalyst	**R^2**	**p**	**R^2**	**p**	**R^2**	**p**	**R^2**	**p**

Mn_3O_4@CoHCF	0.9989	0.003	0.9985	0.04	0.9736	0.001	0.9634	0.001
CoHCF	0.9939	0.02	0.9989	0.02	0.9972	0.001	0.9928	0.003
Mn_3O_4	0.9945	0.01	0.9951	0.01	0.9663	0.002	0.9973	0.002

	DRK				**Freundlich**			
	ET		**CP**		**ET**		**CP**	
Catalyst	**R^2**	**p**	**R^2**	**p**	**R^2**	**P**	**R^2**	**p**
Mn_3O_4@CoHCF	0.9968	0.01	0.9986	0.16	0.9968	0.001	0.9981	0.001
CoHCF	0.9951	0.001	0.9971	0.23	0.9964	0.001	0.9885	0.002
Mn_3O_4	0.9936	0.001	0.9957	0.61	0.9943	0.002	0.9687	0.002

Table 4S: Reduced chi square and Adjusted R square values of kinetics model for ET and CP

	Mn_3O_4@CoHCF			**CoHCF**			**Mn_3O_4**			**Blank**		
Catalyst	**Adj. R^2**	**Red. Chi^2**	**DOF**	**Adj. R^2**	**Red. Chi^2**	**DOF**	**Adj. R^2**	**Red. Chi^2**	**DOF**	**Adj. R^2**	**Red. Chi^2**	**DOF**
ET	0.98016	0.00208	3	0.99643	0.00208	3	0.99533	0.0014	3	0.94004	$5.8* 10^{-4}$	3
CP	0.97573	6.962	3	0.96736	2.291	3	0.99323	1.107	3	0.98324	0.075	3

Table 5S: Reduced chi square and Adj. R square values of kinetics model for ET and CP pollutant.

	Langmuir						Temkin					
	ET			CP			ET			CP		
Catalyst	**Adj. R^2**	**Red. Chi^2**	**DOF**	**Adj. R^2**	**Red. Chi^2**	**DOF**	**Adj. R^2**	**Red. Chi^2**	**DOF**	**Adj. R^2**	**Red. Chi^2**	**DOF**
Mn_3O_4 @CoHCF	0.9989	0.07312	3	0.99801	0.25792	3	0.9649	1.92433	3	0.9649	1.924	3
CoHCF	0.99107	0.06589	3	0.99857	0.19169	3	0.99631	0.31188	3	0.9963	0.31188	3
Mn_3O_4	0.99226	0.06308	3	0.99353	1.12844	3	0.95517	5.16317	3	0.95517	5.16317	3

	DRK						Freundlich					
	ET			CP			ET			CP		
Catalyst	**Adj. R^2**	**Red. Chi^2**	**DOF**	**Adj. R^2**	**Red. Chi^2**	**DOF**	**Adj. R^2**	**Red. Chi^2**	**DOF**	**Adj. R^2**	**Red. Chi^2**	**DOF**
Mn_3O_4 @CoHCF	0.99584	0.38996	3	0.99848	0.3238	3	0.9649	1.924	3	0.997948	0.15618	3

CoHCF	0.99356	0.77154	3	0.9971	1.1935	3	0.99631	0.3118	3	0.98476	2.1225	3
Mn_3O_4	0.99154	1.05498	3	0.9957	1.0299	3	0.9551	5.162	3	0.95835	2.4333	3

Table 6S: Comparison table of different photocatalysts

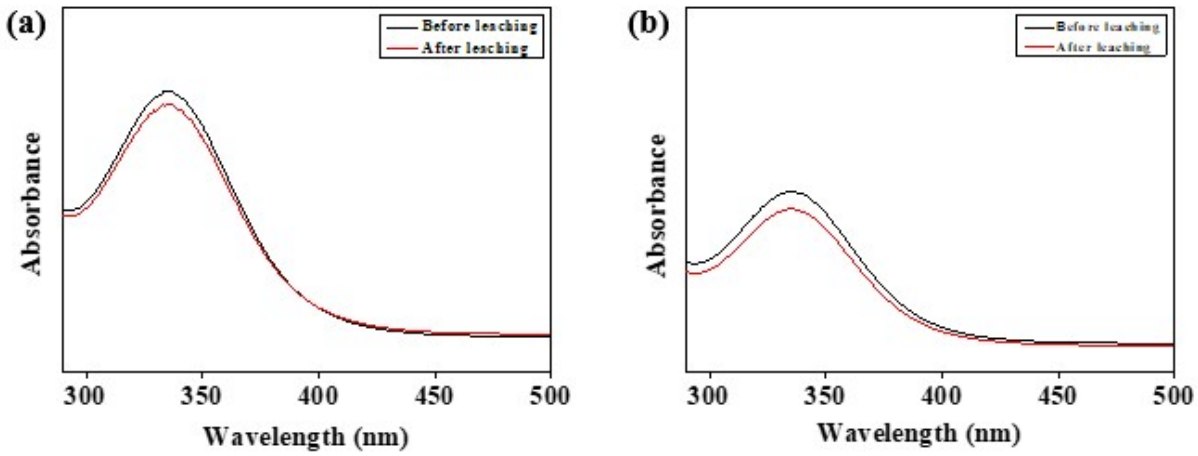

Fig.6S Leaching study in (a)1 N HCl (b) 0.5 N HCl of Mn_3O_4@CoHCF nanocomposite

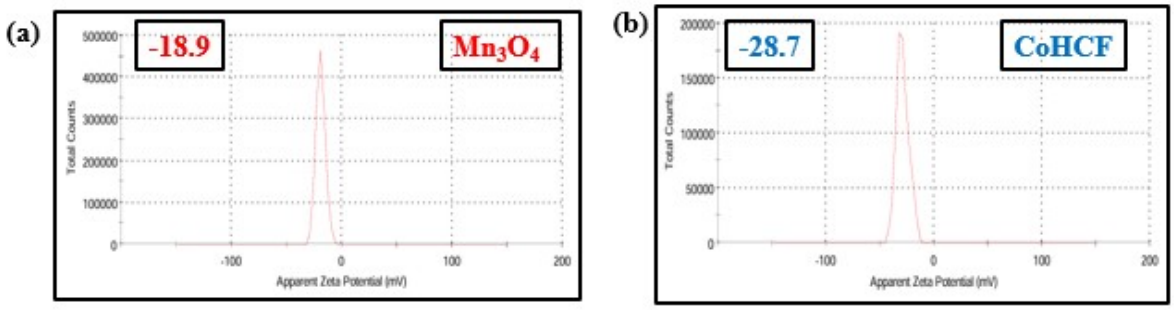

Fig.7S Zeta potential of (a) Mn_3O_4 and (b) CoHCF nanocomposite

References of Table 6S:

Catalyst	**Pollutants**	**Characterization Technique**	**Mechanism and Degradation %**	**Reference**
Zn-Mn_3O_4/TiO_2	Methylene Blue	P-XRD, FTIR, TGA DSC, BET, HRTEM, GC-MS,	Sol-gel method, Photodegradation-96%	[1]
Prussian blue/Mn_3O_4	Levofloxacin	P-XRD, FTIR, FE-SEM, EIS, PL	Z-scheme p-n heterojunction, Photodegradation-96%	[2]

Mn_3O_4@g-C_3N_4	Erythrosine B (EB) Indigo Carmine (IC)	P-XRD, FTIR, Raman, XPS, FE-SEM	Follow pseudo-2nd-order kinetics Photodegradation-92.7%	[3]
Fe_3S_4/Mn_3O_4	Methylene Blue (MB) and Trichlorophenol (TCP)	P-XRD, FTIR, FE-SEM, XPS, BET, TGA	Hydrothermal process, Photodegradation-97.5%	[4]
$CoFe_2O_4/Mn_3O_4$	Methylene Blue	P-XRD, FE-SEM, XPS, FTIR, Raman	Sol-gel-cum- hydrothermal method, LEDdriven photocatalysis -92%	[5]
Mn_3O_4/ZnO	Tetracycline	P-XRD, FTIR, FE-SEM, BET, XPS	Ultrasonification, Photodegradation-97.5 %	[6]
$ZrTiO_4/TiO_2$/ Mn_3O_4 (ZTM)	Metoclopramide (MCP)	P-XRD, FTIR, UV–Vis DRS, EIS, TG/DTG, SEM, TEM	Z-scheme charge transfer, Photodegradation-97.5 %	[7]
Al_2O_3/Mn_3O_4/ Fe_2O_3	Methylene Blue	P-XRD, FTIR, SEM-EDS	Co-precipitation method, UV-radiation 98.2%	[8]
NiO/Mn_3O_4	Thiamethoxam, crystal violet, rhodamine B	P-XRD,FTIR, FE-SEM, EDS, XPS, HR-TEM	Hydrothermal method, Photocatalytic degradation -93% ,93.6%, 93.2%	[9]
Ag/Mn_3O_4	Congo red	P-XRD,XRF,Raman, BET, SEM, TEM	Sol–gel and hydrothermal methods, Sonophotocatalytic degradation	[10]
Mn_3O_4@CoHCF	Ethion (ET) and Chlorpyrifos (CP)	P-XRD,FTIR, FE-SEM, XPS, BET, ESR	Photocatalytic degradation	Present Work

References

[1] Syed Aminullah, Safia Hassan Mohammed M. Alanazi, Zahid Imran , Liaqat Rasheed, Sumra Afzal, Wajid Rehman, Solar light driven boost photocatalytic activity and tailoring bandgap of Zn-Mn_3O_4/TiO_2 a hetero-structures for degradation of organic dyes, J. Alloys Compd., 2025,**1027**, 180436.

[2] Fenfen Xi, Mengyuan Yue, Jinhui Zhao, Kongliang Xie, Jianfeng Ma, Xiyu Songc, Liping Lianga, Aiqin Houa, Photo-Fenton enhanced self-floating Z-scheme Prussian blue/Mn_3O_4 heterojunction for efficient levofloxacin degradation: Mechanism, pathway and DFT analysis, Colloid. Surf. A Physicochem. Eng. Asp.,2026,**728**, 138653.

[3] Afroja Banua, Suranjan Sikdar, Sonia Agrawal, Biswajit Sinha, Mn_3O_4 based g-C_3N_4 nanocomposite used for the photodegradation of Erythrosine B and Indigo Carmine dyes and its effects on cell viability, J. Water Process Eng.,2026,**86**, 109824.

[4] Haya Alhummiany, Design of S-scheme Fe_3S_4/Mn_3O_4 magnetic nanocomposites as photo-Fenton-like catalysts for efficient pollutant degradation, J. Phys. Chem. Solids, 2025, **207**, 112845.

[5] Vidit Pandey, Sandeep Munjal, Tufail Ahmad, Visible LED-light driven photocatalytic activity by a novel magnetically separable $CoFe_2O_4$/Mn_3O_4 nanocomposite, Nano-Structures & Nano-Objects, 2024,**40**,101351.

[6] M.S. Amin,F.M. Alshareef, Wejdan T. Alsagg Employing manufactured Mn_3O_4–ZnO nanocomposite for ameliorated photocatalytic performance under visible light, Optical Materials, 2022,**127**,112286.

[7]Razieh Fazaelia,HamidAliyanb,AlirezaNezamzadeh-Ejhiehb,DarrinRicheson Investigation of the synergistic photocatalytic activity of a ternary $ZrTiO_4$/ TiO_2/Mn_3O_4(ZTM) nanocomposite in a typical water treatment process , **Surf. Interfaces.,**2024,**52**, 104877.

[8] Rahul Sharma, Harish Kumar, Chetna Saini, Anu Gupta, Vaidehi Pandit, Exploring the collaborative wonders of Al_2O_3-Mn_3O_4-Fe_2O_3 nanoparticles embedded in reduced graphene oxide matrices, 2023,**157**,11135.

[9] Mandvi, Prit Pal Singh, Suhas Ballal, Mamta Chahar, Jaya Bansal, Ranvijay Kumar, Sandeep Kumar and Sandeep Kaushal Construction of a 3D flower-like NiO/Mn_3O_4 heterojunction using Tulsi leaf extract for enhanced photodegradation of thiamethoxam pesticide and organic dyes under direct sunlight, Mater. Adv., 2024, **5**, 8097.

[10] Muhammad Yose Rizala, Rosari Saleha, Suhendro Purbo Prakoso, Ardiansyah Taufike, Shu Yine Ultraviolet- and visible-light photocatalytic and sonophotocatalytic activities toward Congo red degradation using Ag/Mn_3O_4 nanocomposites,2021,**121**, 105371.